Stem Cell Reports
Report
ISSCR
OPEN ACCESS

Attrition of X Chromosome Inactivation in Aged Hematopoietic Stem Cells

Ani Grigoryan,[1,11] Johannes Pospiech,[1] Stephen Krämer,[2,3,4,5] Daniel Lipka,[2] Thomas Liehr,[6] Hartmut Geiger,[1] Hiroshi Kimura,[7] Medhanie A. Mulaw,[1,8,*] and Maria Carolina Florian[1,9,10,12,*]

[1]Institute of Molecular Medicine and Stem Cell Aging, University of Ulm, Albert-Einstein-Allee 11c, 89081 Ulm, Germany
[2]Section Translational Cancer Epigenomics, Division of Translational Medical Oncology, German Cancer Research Center (DKFZ) & National Center for Tumor Diseases (NCT) Heidelberg, Heidelberg, Germany
[3]Bioinformatics and Omics Data Analysis, German Cancer Research Center (DKFZ), Heidelberg, Germany
[4]Faculty of Biosciences, University of Heidelberg, Heidelberg, Germany
[5]Biomedical Informatics, Data Mining and Data Analytics, Faculty of Applied Computer Science and Medical Faculty, University of Augsburg, Augsburg, Germany
[6]Jena University Hospital, Friedrich Schiller University, Institute of Human Genetics, Am Klinikum 1, 07747 Jena, Germany
[7]Cell Biology Center, Institute of Innovative Research, Tokyo Institute of Technology, 4259 Nagatsuta-cho, Midori-ku, Yokohama 226-8503, Japan
[8]Department of Internal Medicine I, University Hospital Ulm, Ulm, Germany
[9]Stem Cell Aging Group, Regenerative Medicine Program, Bellvitge Institute for Biomedical Research (IDIBELL) and Program for advancing the Clinical Translation of Regenerative Medicine of Catalonia, P-CMR[C], Av. Gran Via 199-203, 08908, L'Hospitalet de Llobregat, Barcelona, Spain
[10]Center for Networked Biomedical Research on Bioengineering, Biomaterials and Nanomedicine (CIBER-BBN), Madrid, Spain
[11]Present address: Laboratory for Cell, Tissue and Organ Engineering, Department of Clinical Sciences, Wallenberg Center for Molecular Medicine, and Stem Cell Center, Lund University, Sölvegatan 19, 221 84 Lund, Sweden
[12]Lead contact
*Correspondence: medhanie.mulaw@uni-ulm.de (M.A.M.), mflorian@idibell.cat (M.C.F.)
https://doi.org/10.1016/j.stemcr.2021.03.007

SUMMARY

During X chromosome inactivation (XCI), the inactive X chromosome (Xi) is recruited to the nuclear lamina at the nuclear periphery. Beside X chromosome reactivation resulting in a highly penetrant aging-like hematopoietic malignancy, little is known about XCI in aged hematopoietic stem cells (HSCs). Here, we demonstrate that LaminA/C defines a distinct repressive nuclear compartment for XCI in young HSCs, and its reduction in aged HSCs correlates with an impairment in the overall control of XCI. Integrated omics analyses reveal higher variation in gene expression, global hypomethylation, and significantly increased chromatin accessibility on the X chromosome (Chr X) in aged HSCs. In summary, our data support the role of LaminA/C in the establishment of a special repressive compartment for XCI in HSCs, which is impaired upon aging.

INTRODUCTION

In eukaryotic cell nuclei, chromatin is highly compartmentalized and euchromatin occupies the interior of the nucleus, while heterochromatin is located around the nucleoli and predominantly at the nuclear periphery associated with lamins (Figure S1A) (Politz et al., 2013; Solovei et al., 2009; van Steensel and Belmont, 2017; Wilson and Berk, 2010). Nuclear lamins are type V intermediate filaments separated into two major classes: A (LaminA and LaminC) and B types (LaminB1 and LaminB2) (Burke and Stewart, 2013; Dechat et al., 2008). LaminA/C (encoded by the *Lmna* gene) deficiency results in the loss of the peripheral heterochromatin silencing compartment (Solovei et al., 2013). Also, it is known that the mammalian Chr X is recruited to the nuclear lamina during X chromosome inactivation (XCI) (Chen et al., 2016). XCI is a process that involves the transcriptional silencing of one Chr X in cells of female mammals to balance gene expression between XX females and XY males by embryonic day 6.5 (E6.5) (Brockdorff et al., 2020; Fang et al., 2019; Galupa and Heard, 2018; Lebon et al., 1995; Loda and Heard, 2019). The silencing of the Xi is regulated by the long non-coding RNA (lncRNA) Xist (Brown et al., 1992; Marahrens et al., 1998; Penny et al., 1996; Sahakyan et al., 2018), which coats the future Xi and then recruits repressive complexes (Chaumeil et al., 2006; da Rocha and Heard, 2017; Engreitz et al., 2013; McHugh et al., 2015; Minajigi et al., 2015; Pandya-Jones and Plath, 2016; Pinheiro and Heard, 2017). In addition to the essential role of Xist in embryonic development, Xist-mediated gene silencing in hematopoietic cells is critical for postnatal survival in mice (Savarese et al., 2006; Yildirim et al., 2013). Notably, the deletion of *Xist* in hematopoietic stem cells (HSCs) after XCI establishment (as HSCs develop at E10.5) causes a highly penetrant aging-like hematopoietic malignancy (Dzierzak and Bigas, 2018; Sahakyan et al., 2016; Yildirim et al., 2013; Yokomizo and Dzierzak, 2010), implying the critical role of Xist in the maintenance of XCI postnatally. However, little is known about XCI in HSC aging.

RESULTS

The Repressive Nuclear Compartment for XCI Is Dependent on LaminA/C and Is Impaired upon HSC Aging

LaminA/C is located at the invaginations of young HSC nuclei forming pocket-like structures around the cytoplasmic tubulin pole (Figure 1A) (Grigoryan et al.,

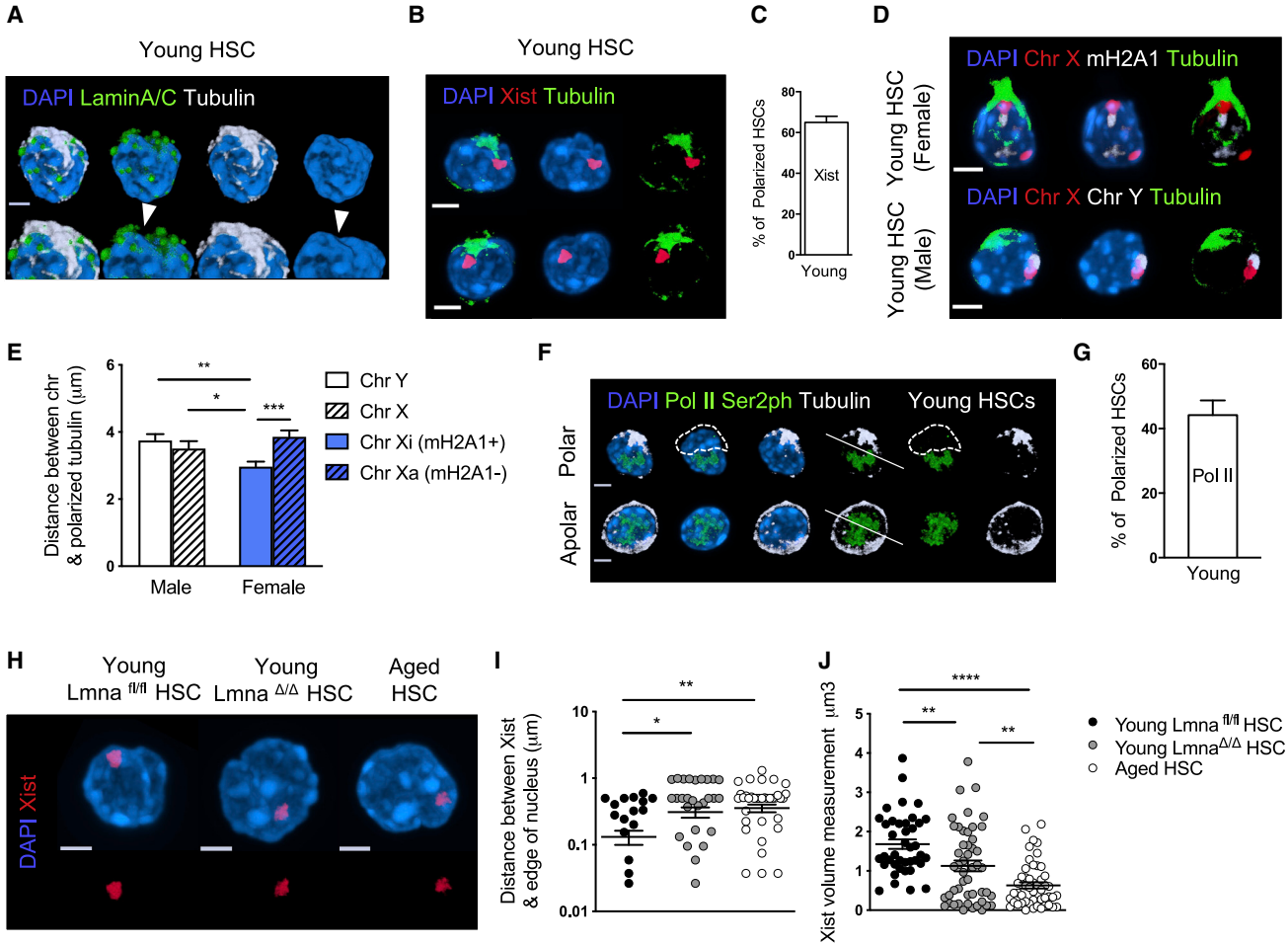

Figure 1. The Repressive Nuclear Compartment for XCI Is Dependent on LaminA/C and Is Impaired upon HSC Aging

(A) 3D reconstruction of LaminA/C (green) and tubulin (white) in young HSCs. Bar, 2 µm. Arrowheads indicate the deep nuclear (blue) invagination often seen in young HSCs.

(B) 3D reconstruction of Xist (red) and tubulin (green) in HSC nuclei (blue) from young female mice. Bar, 2 µm.

(C) Percentage of young HSCs with localization of Xist close to tubulin pole. Shown are mean values + 1 SE; n = 4, total 85 cells

(D) 3D reconstruction of Chr X/Y (red and white), Chr X/X (red), mH2A1 (white), and tubulin (green) in HSC nuclei (blue) from young female and male mice. Bar, 2 µm.

(E) Measurements of the distances between Chr X/Y and tubulin, Chr X/X, and tubulin in young male and female HSCs; *p < 0.05; **p < 0.01; ***p < 0.001; n = 3 male mice, total 33 cells; n = 5 female mice, total 47 cells. Shown are mean values + SE.

(F) 3D reconstruction of Pol II Ser2ph (green) and tubulin (white) in polar and apolar HSC nuclei (blue) from young female mice. Bar, 2 µm. The selected area depicts Pol II Ser2ph depleted region in young HSCs. Lines are drawn to show polar and apolar distribution of Pol II Ser2ph.

(G) Percentage of young HSCs with a polar distribution of Pol II Ser2ph. Shown are mean values + 1 SE; n = 4, total 50 cells.

(H) 3D reconstruction of Xist (red) stained by RNA-FISH in HSCs (blue) of young (10-week-old) female *Lmna*$^{fl/fl}$ control and *Lmna*$^{\Delta/\Delta/Vav-Cre}$ mice and aged (90-week-old) female mice. Bar, 2 µm.

(I and J) Xist distance from the edge of the nucleus and Xist volume measurements, based on Xist staining as depicted in (H); *p < 0.05; **p < 0.01; ****p < 0.0001; n = 3, total 40 cells for *Lmna*$^{fl/fl}$ control mice; 49 cells for *Lmna*$^{\Delta/\Delta/Vav-Cre}$ mice; 48 cells for aged mice. Shown are mean values +SE.

See also Figure S1.

2018). Thus, we hypothesized that the peculiar and specific 3D localization of LaminA/C in young HSCs might establish a distinct repressive compartment for XCI.

To characterize the LaminA/C-tubulin pole as a repressive nuclear compartment in young HSCs (as described in the experimental proceduressection), we investigated the 3D localization of Xist by single-HSC RNA fluorescence *in*

situ hybridization (RNA-FISH). In these cells, Xist was located at the nuclear invagination close to the LaminA/C-tubulin pole (Figures 1B, 1C, and S1B). Next, we analyzed Chr Xa/Xi (active and inactive) and Chr X/Y co-distribution relative to the LaminA/C-tubulin pole in young female and male HSC nuclei respectively (Figures 1D and 1E). To distinguish Xi and Xa in female HSCs, we used the repressive macro H2A histone variant 1 (mH2A1), which accumulates on the Xi during XCI (Figure S1C) (Costanzi and Pehrson, 1998; Pandya-Jones and Plath, 2016; Plath et al., 2002). Immunofluorescence in combination with DNA-FISH analysis for the whole Chr X consistently showed that the Xi (mH2A1+) was located significantly closer to the LaminA/C-tubulin pole than the Xa (mH2A1−) in female and also compared with the Chr X and Y in male HSCs (Figures 1D, 1E, and S1D).

Rapid depletion of RNA polymerase II (Pol II) is one of the first steps during XCI (Chaumeil et al., 2006; McHugh et al., 2015). Interestingly, we observed that Pol II Ser2ph (phosphorylated at serine 2) is depleted at the LaminA/C-tubulin pole, showing a polarized localization at the opposite side of the nucleus, where the active marker H4K16ac was observed (Figures 1F, 1G, S1E, and S1F) (Florian et al., 2012). Collectively, these data imply that the LaminA/C-tubulin pole might possibly define a distinct repressive compartment for the Xi at one side of the nucleus, which is separated from the other active compartment of the HSC nucleus (Figure S1G).

With aging, the activity of HSCs decreases, resulting in impaired tissue homeostasis, reduced engraftment following transplantation, and increased susceptibility to myeloproliferative diseases (with higher incidence of acute myeloid leukemia and myelodysplastic syndromes [MDSs]) (Akunuru and Geiger, 2016; Beerman et al., 2010; Denkinger et al., 2015; Geiger et al., 2013; Guidi and Geiger, 2017; Rossi et al., 2007; Snoeck, 2013). Since we recently reported the decrease of LaminA/C expression as an additional phenotype of aged HSCs (Grigoryan et al., 2018), we asked whether this could affect the repressive nuclear compartment for XCI in aged HSCs. To causally link LaminA/C expression to XCI, we analyzed young HSCs from mice lacking LaminA/C specifically in the hematopoietic compartment ($Lmna^{\Delta/\Delta/Vav-Cre}$) in parallel to aged HSCs (Grigoryan et al., 2018; Wang et al., 2015). Interestingly, Xist was significantly further away from the edge of the nucleus, and the 3D volume of Xist detected by RNA-FISH was significantly decreased in $Lmna^{\Delta/\Delta/Vav-Cre}$ and aged HSCs compared with young control HSCs (Figures 1H–1J). These data indicate a likely alteration of Xist localization at the LaminA/C peripheral repressive compartment, implying that the loss of LaminA/C is linked to the reduction of Xist expression in HSCs upon aging.

The XCI Is Impaired upon HSC Aging

Xist expression was significantly reduced by RT-PCR in aged HSCs compared with young HSCs and it remained significantly decreased in more differentiated aged short-term HSCs (ST-HSCs) compared with young ST-HSCs (Figures 2A and 2B).

To gain further insights into possible X-linked gene expression alterations upon aging, we analyzed RNA sequencing (RNA-seq) datasets from young and aged HSCs and ST-HSCs (Grigoryan et al., 2018). Although there were no significant differences in X-linked gene expression across all samples (Figure 2C), we could observe a higher gene expression variability along Chr X in aged HSCs compared with young samples (Figure 2C). Indeed, as can be noted in Figure 2C, the running mean difference of gene expression profile along Chr X shows subtle or no deviation from zero in the young samples, while the aged samples show higher variability. This implies that there is higher gene expression variation in X-linked genes among aged samples than young ones. Although not conclusive regarding reactivation of Chr X upon aging and limited to only three biological replicates per sample, this result supports a higher overall transcriptional variation and activity on Chr X in aged HSCs in contrast to their young counterparts.

To understand if the increased heterogeneity of X-linked gene expression observed in bulk aged HSCs is allele specific, we performed an allele-specific expression analysis using previously published single-cell RNA-seq (scRNA-seq) data of young and aged HSCs (Florian et al., 2018). This approach allows us to overcome the averaging-out effect that typically exists in bulk cell analysis and thus provides a more accurate profile of the allele-specific quantification. Also, it provides significant statistical power as each cell is analyzed independently and summarization across age groups is based on hundreds of single cells.

Therefore, for each single cell, first we counted the number of reads covering high-confidence heterozygous single nucleotide variants (SNVs) according to the murine database of SNP(dbSNP; see experimental procedures section for details) (Figure 2D upper panel). A correlation analysis of the distribution of SNV/SNP on both alleles (i.e., the reference allele, which is the allelic state as annotated in the reference genome, versus the alternate allele) was then performed to assess the overall allelic representation frequency (Figure 2D upper and lower left panel depict a representative plot showing respectively weak and strong correlation between reference and major Chr X alleles of a given cell). We observed that the median Kendall's correlation coefficients were approximately 0.4 and −0.3 for reference and alternate allele respectively, indicating that the major allele is primarily represented by the reference allele (Figure 2D lower left panel). We also confirmed that there is no

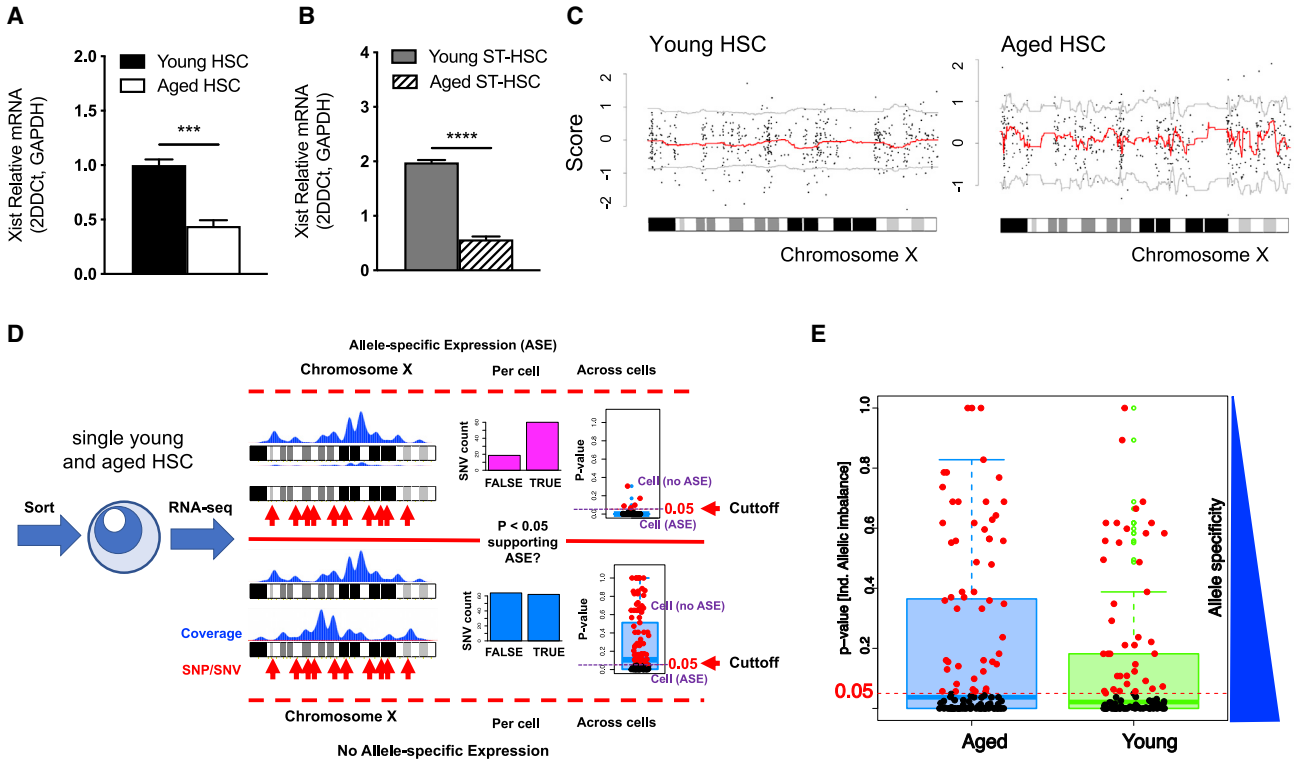

Figure 2. The XCI Is Impaired upon HSC Aging

(A and B) *Xist* transcript levels in young and aged female HSCs and ST-HSCs measured by RT-PCR. Shown are mean values + 1 SE; n = 3; ***p < 0.001.

(C) MACAT analysis showing differentially regulated genes on Chr X. Gene expression patterns for all four arms are shown. Y axis shows fold differential regulation when HSCs were compared with ST-HSCs in young and in aged samples. Positive values indicate upregulation, while negative values indicate downregulation. Dots represent individual genes. Gray lines indicate the minimum score for differential gene expression and the red line indicates the level of differential regulation of genes along Chr X.

(D) Diagram showing the scRNA-seq allele-specific expression (ASE) analysis workflow. See experimental procedures section for details.

(E) Boxplot showing ASE profile in young (green) and aged (blue) HSC single cells (red points). Cutoff of significance (supporting ASE) is shown by the dotted red line (p value < 0.05). Blue triangle on right side highlight that the closer cells are to zero along the y axis, the higher the evidence supporting ASE. A test of the proportion of aged HSCs with no significant ASE was statistically significant (p value 0.0003085, χ^2 test = 13.018, df = 1).

See also Figure S1 and Table S1.

statistically significant difference in major allele representation between the age groups (Figure 2D lower left panel).

Finally, we assessed if the frequency of SNPs per cell supporting allele-specific expression is significantly higher or lower than those indicating no allele specificity (Figure 2D lower right panel). Goodness-of-fit test was used to reach a decision on whether Chr X data for a given cell support allele-specific expression (Table S1; significant p value indicates allele-specific expression significance). By comparing the number of young and aged single cells supporting allele-specific expression, the data show a higher proportion of aged stem cells with no significant allele-specific expression compared with young HSCs (Figure 2D lower right panel, 2E and S1H), supporting overall an impairment in XCI in aged stem cells.

Assay for Transposase-Accessible Chromatin Sequencing Profiling Shows the Epigenetic Deregulation of Chr X in Aged HSCs

Xist expression and consequently XCI are mainly regulated by epigenetic mechanisms (Panning and Jaenisch, 1998). Since HSCs undergo an epigenetic drift upon aging (Beerman et al., 2013; Florian et al., 2018; Grigoryan et al., 2018; Mejia-Ramirez et al., 2020; Sun et al., 2014; Taiwo et al., 2013), we hypothesized that epigenetic alterations might underlie the changes in XCI upon HSC aging.

Xist expression is controlled by DNA methylation at specific CpGs (Plath et al., 2002). To investigate whether the epigenetic regulation of XCI is altered in aged HSCs, we generated a tagmentation-based whole-genome bisulfite sequencing (TWGBS) dataset. Chr X methylation levels

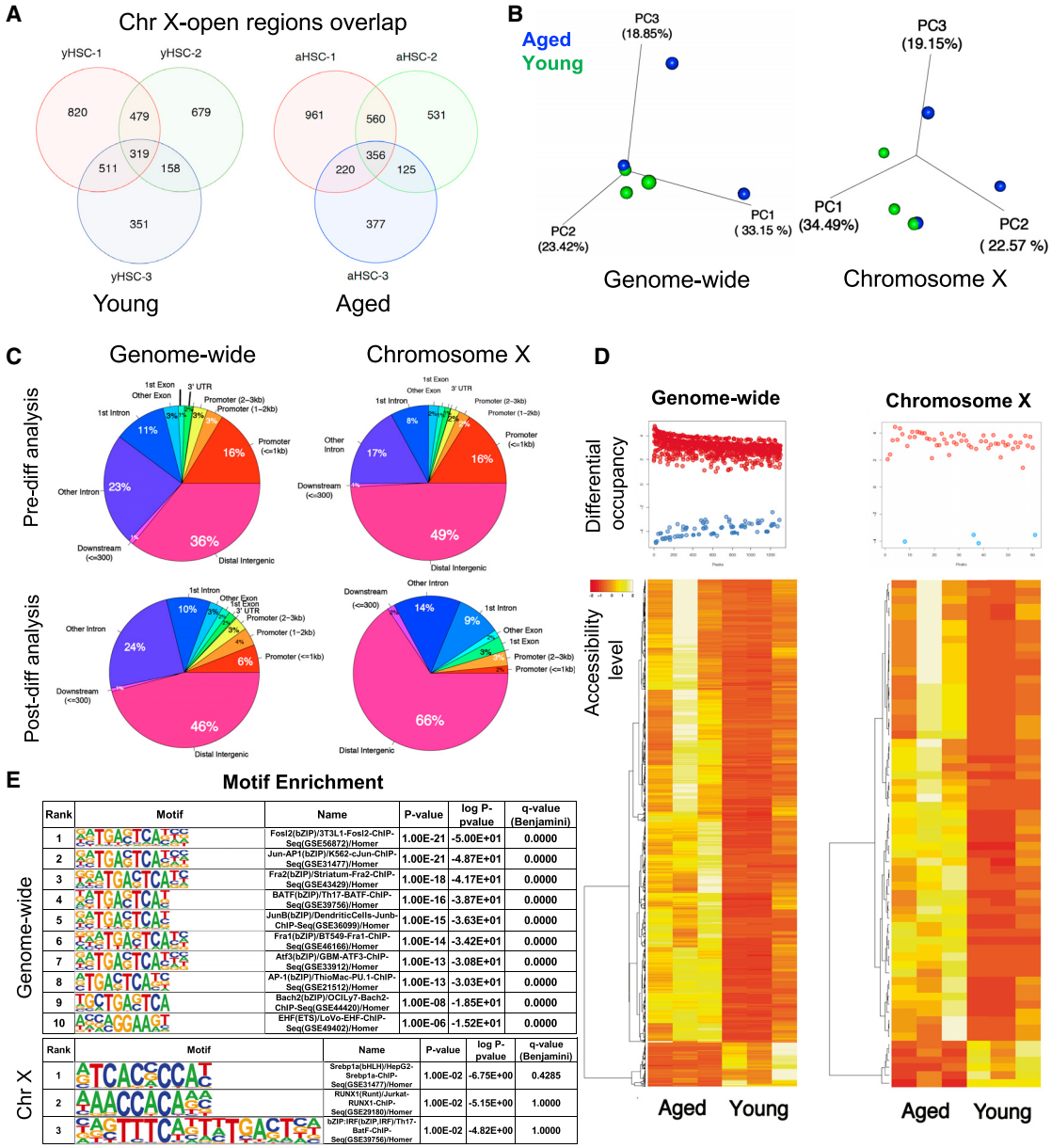

Rank	Motif	Name	P-value	log P-pvalue	q-value (Benjamini)
1		Fosl2(bZIP)/3T3L1-Fosl2-ChIP-Seq(GSE56872)/Homer	1.00E-21	-5.00E+01	0.0000
2		Jun-AP1(bZIP)/K562-cJun-ChIP-Seq(GSE31477)/Homer	1.00E-21	-4.87E+01	0.0000
3		Fra2(bZIP)/Striatum-Fra2-ChIP-Seq(GSE43429)/Homer	1.00E-18	-4.17E+01	0.0000
4		BATF(bZIP)/Th17-BATF-ChIP-Seq(GSE39756)/Homer	1.00E-16	-3.87E+01	0.0000
5		JunB(bZIP)/DendriticCells-JunB-ChIP-Seq(GSE36099)/Homer	1.00E-15	-3.63E+01	0.0000
6		Fra1(bZIP)/BT549-Fra1-ChIP-Seq(GSE46166)/Homer	1.00E-14	-3.42E+01	0.0000
7		Atf3(bZIP)/GBM-ATF3-ChIP-Seq(GSE33912)/Homer	1.00E-13	-3.08E+01	0.0000
8		AP-1(bZIP)/ThioMac-PU.1-ChIP-Seq(GSE21512)/Homer	1.00E-13	-3.03E+01	0.0000
9		Bach2(bZIP)/OCILy7-Bach2-ChIP-Seq(GSE44420)/Homer	1.00E-08	-1.85E+01	0.0000
10		EHF(ETS)/LoVo-EHF-ChIP-Seq(GSE49402)/Homer	1.00E-06	-1.52E+01	0.0000

Rank	Motif	Name	P-value	log P-pvalue	q-value (Benjamini)
1		Srebp1a(bHLH)/HepG2-Srebp1a-ChIP-Seq(GSE31477)/Homer	1.00E-02	-6.75E+00	0.4285
2		RUNX1(Runt)/Jurkat-RUNX1-ChIP-Seq(GSE29180)/Homer	1.00E-02	-5.15E+00	1.0000
3		bZIP:IRF(bZIP:IRF)/Th17-BatF-ChIP-Seq(GSE39756)/Homer	1.00E-02	-4.82E+00	1.0000

P-value	ln(P)	Term	GO Tree	Genes in Term	Target Genes in Term	Total Genes	Target Genes	Common Genes
7.73E-09	-18.68	chrxp22	MSigDB lists	80	6	15720	30	Mospd2,Pdha1,Arhgap6, Rps6ka3,Sh3kbp1,Nhs
3.21E-08	-17.26	chrxq13	MSigDB lists	49	5	15720	30	Pja1,Zdhhc15,Cysltr1, Pcdh19,Stard8
2.85E-07	-15.07	mouse chrX|X F5	chromosome location	24	4	24177	57	Arhgap6,Mospd2, Rnf138rt1,Gm8817
6.08E-07	-14.31	chrxq21	MSigDB lists	36	4	15720	30	Pabpc5,Tgif2lx2,Pcdh19, Dach2
2.02E-06	-13.11	mouse chrX|X A4	chromosome location	11	3	24177	57	4930515L19Rik,Prr32, Tex13c1
5.54E-06	-12.1	mouse chrX|X B	chromosome location	15	3	24177	57	Prrg1,Gm14743,Gm8787
1.08E-05	-11.43	chrxq24	MSigDB lists	23	3	15720	30	Il13ra1,C1galt1c1,Lrch2
1.40E-05	-11.18	mouse chrX|X D	chromosome location	62	4	24177	57	Gm732,Cysltr1,Zdhhc15, Mir384
1.60E-05	-11.04	mouse chrX|X F2	chromosome location	21	3	24177	57	Amot,Pak3,Lrch2
2.22E-05	-10.72	GAUSSMANN_MLL_AF4_FUSION_TARGETS_G_DN	MSigDB lists	29	3	15720	30	Lrch2,Rnf128,Mtm1

Figure 3. ATAC-Seq Profiling Shows the Epigenetic Deregulation of Chr X in Aged HSCs

(A) Venn diagrams showing ATAC-seq peaks overlap between biological replicates of young (left) and aged (right) samples.

(B) PCA based on ATAC-seq peaks feature counts both genome-wide (left) and Chr X-specific (left) peaks, which shows segregation of young and aged samples. In detail, the data display the intra-cluster distance between the samples (i.e., how far apart the aged samples are from each other compared with the relative distance between the young samples).

(legend continued on next page)

remained comparatively unchanged upon HSC aging and we observed a significant correlation between young and aged samples' methylation profiles along Chr X (Figure S2A). The Xist promoter was also not differentially methylated in young compared with aged samples (Figure S2B). To further assess if there was any variation in the methylation levels between young and aged HSCs, we looked at the distribution of the methylation profiles and their corresponding standard deviations along Chr X in young and aged HSCs, but did not observe significant difference between samples (Figures S2C and S2D). Indeed, the variability of the methylation level on Chr X in young and aged HSCs was similar and did not match the increased transcriptional variability observed for the transcriptome of aged HSCs (Figure 2C). Then, we performed principal component analysis (PCA) based selectively on Chr X methylation. Interestingly, the top three principal components (PCs) revealed that aging is indeed a primary source of variation, and we observed by this approach a separation of young and aged HSCs based solely on Chr X methylation profiles (Figure S2E). We then performed Chr X-based differential methylation analysis and identified 5,835 differentially methylated regions (DMRs) at a q-cutoff value of 0.05, of which 113 had a mean difference greater than or equal to 0.1 with at least three methylation marks representing them (Table S2 and Figure S2F). Genomic annotation of the DMRs revealed that genomic regions were largely hypomethylated in aged HSCs compared with young HSCs (Figure S2G). These data would support that Chr X in aged HSCs, in addition to hypomethylation in intergenic regions, might be more transcriptionally permissive compared with young HSCs.

To further dig into the epigenetics of the alterations in XCI skewing upon HSC aging, and in particular to link the observations of decreased Xist expression (Figures 1J and 2A) to the change from a peripheral to a central nuclear location upon decreased LaminA/C expression and aging (Figures 1H and 1I), we performed assay for transposase-accessible chromatin sequencing (ATAC-seq) (Buenrostro et al., 2015; Giorgetti et al., 2016). ATAC-seq can offer a readout of chromatin architecture accessibility, which is more directly linked to the control of transcription (Liu et al., 2019), and it readily reflects changes in HSC function upon aging (Florian et al., 2018). Our data on bulk sorted young and aged HSCs revealed that, while globally there is a higher amount of open chromatin regions in aged HSCs (Figure S2H), the overall number of reproducible peaks (across biological replicates) representing open regions along Chr X were fairly equal in amount between samples (356 for aged and 319 for young HSCs; Table S3 and Figure 3A). PCA based on the genome-wide peaks segregated the two age groups into distinct clusters (Figure 3B). Also, aged HSCs showed a higher heterogeneity compared with young HSCs (Figure 3B, left panel; cumulative explained variance $\approx$75%). In line with the genome-wide findings, PCA based on Chr X peak sets also separated the two age groups (Figure 3B; cumulative explained variance $\approx$76%). We then performed differential occupancy analysis and identified 1,302 (genome-wide) and 64 (Chr X-specific) statistically significant ATAC-seq different accessible regions (DARs) (p value <0.05) (Table S4). By looking at the genomic regions' distributions of the signal before and after differential analysis, we noticed that both genome-wide and Chr X-specific peaks show predominant enrichment in the same region sub-types (distal intergenic, intronic [other intron], promoter [$\leq$ 1 kb], and first intronic regions; Figure 3C). Interestingly, compared with the pre-differential analysis, Chr X-specific DARs increased dramatically in the proportions of distal intergenic (from 49% to 66%) and decreased at promoter ($\leq$1 kb) (from 16% to 2%) regions (Figure 3C, lower right panels). Overall, most of the DARs (both genome-wide and Chr X-specific DARs) predominantly fall in distal intergenic and affect promoters only minimally.

Notably, 91% (1,186/1,302) of genome-wide DARs in aged HSCs were open regions, which is statistically highly significant against the null hypothesis of equal representation of open and closed regions (χ^2 = 879.34; p value < 0.001; Figure 3D). Similarly, we observed a statistically significant over-representation of open DARs (90.6% or 58 out of 64) along Chr X (χ^2 = 42.25; p value < 0.001; Figures 3D and S2I).

Finally, we performed motif and gene ontology (GO) enrichment analyses on DARs. Although we could see statistically significant enrichment of various motifs

(C) Distribution of ATAC-seq peaks by genomic regions. Analysis at the genome level (left panel) and Chr X (right panel) shows predominant enrichment in distal intergenic, intronic, and promoter ($\leq$ 1kb) regions. Differential analysis (lower panels) revealed Chr X-specific DARs increase in the proportion of distal intergenic peaks and a reduction in the promoter ($\leq$1 kb) regions.

(D) Genome-wide and Chr X-specific differential peak occupancy/accessibility. Red points on the scatterplots (upper panels) show differentially accessible regions (open in aged HSCs), while blue points show those that are more accessible in the young samples (yellow = higher fold change; orange/red = lower fold change or lower accessibility in the samples indicated below).

(E) Tables depicting motif enrichment analysis using HOMER.

(F) Table showing statistically significantly enriched chromosomal regions and gene signatures associated with Chr X (based on HOMER GO analysis of Chr X DARs). The associated p values are shown in the first column.

See also Figure S2 and Tables S2, S3, and S4.

associated with transcription factors for whole-genome DARs (Figure 3E, for top 10), we saw enrichment of Srebp1, RUNX1, and bZIP:IRF motifs along Chr X, although that was not significant ($p < 0.05$; q value [BH: Benjamini-Hochberg] not significant; Figure 3E). This lack of enrichment in transcription factors' motifs was not surprising, since more than 90% of the DARs along Chr X fall into either distal intergenic or intronic regions (Figure 3C, lower right panels). In line with this, GO analysis of Chr X-specific DARs primarily showed enrichment of terms related to position rather than function (Figure 3F, for top 10 significant sets), further strengthening the possibility that the open chromatin distribution changes on Chr X reveal mainly chromatin architectural alterations in HSCs upon aging.

DISCUSSION

Altogether, these data demonstrate that LaminA/C defines a polar repressive compartment for XCI in young HSC nuclei and its reduction in aged HSCs correlates with an impairment in the overall control of the Xi localization and inactivation. These alterations are known to be critical for XCI (Galupa and Heard, 2018) and in HSCs they appear to be rather general to the whole Chr X and not gene specific.

The omics datasets support that, upon HSC aging, whole-genome chromatin accessibility increases, also affecting Chr X. These findings imply that many regions on Chr X are significantly more accessible in aged HSCs compared with young. Indeed, our data also support an increased transcriptional activity and higher heterogeneity in Chr X gene expression in aged HSCs compared with young stem cells. Surprisingly, this increased accessibility does not appear to be specific to any transcription factor, gene, pathway, or direct molecular function and instead seems to be linked to structural alterations in Chr X architecture. The observation of increased accessibility supports the view of a general relocalization of the Xi to a more active region of the nucleus and decreased Xist levels. In addition, based on the TWGBS dataset, we observed that promoter regions on Chr X of aged samples show hypomethylation, further supporting the enhanced accessibility and transcriptional heterogeneity of this Chr in aged HSCs. In summary, our findings altogether argue that Chr X is epigenetically deregulated in aged HSC samples and that this epigenetic deregulation is mainly associated to a change in localization and a disruption in nuclear compartmentalization in aged HSCs.

Interestingly, deregulation of XCI in the hematopoietic compartment causes an aging-like MDS with 100% penetrance in mice (Yildirim et al., 2013). Therefore, the existence of an age-dependent alteration of XCI may raise important implications for understanding the physiology of hematopoiesis during aging and the pathogenesis of age-related hematopoietic malignancies. Interestingly, we report here that the chromatin architecture (ATAC-seq dataset) senses this change in XCI upon HSC aging and this aspect might deserve further attention, since it could offer possibilities to dissect the epigenetic changes underlying aging and disease in the hematopoietic system.

Further studies are needed to unravel mechanistically which of these epigenetic components might be more relevant to drive the enhanced disease predisposition in aged HSCs.

EXPERIMENTAL PROCEDURES

Mice

C57BL/6 mice (2–4 months old) were obtained from Janvier. Aged C57BL/6 mice (20–26 months old) were obtained from the internal divisional stock (derived from mice obtained from both The Jackson Laboratory and Janvier) as well as from NIA/Charles River. Congenic C57BL/6.SJL-Ptprca/Boy (BoyJ) mice were obtained from Charles River Laboratories or from the internal divisional stock (derived from mice obtained from Charles River Laboratories). To obtain the hematopoietic-specific knock out of LaminA/C, the Lmna flox mice (kindly provided by Dr. C. Stewart; Wang et al., 2015) were crossed with mice bearing the hematopoietic specific Vav-Cre transgene (B6.Cg-Tg (Vav1-Cre) A2Kio/J) (Croker et al., 2004; Grigoryan et al., 2018; Wang et al., 2015). All mice were housed in the animal barrier facility under pathogen-free conditions either at the University of Ulm or at CCHMC. All mouse experiments were performed in compliance with the German Law for Welfare of Laboratory Animals and were approved by the Institutional Review Board of the University of Ulm and by the Regierungspräsidium Tübingen.

Cell Isolation

Bone marrow mononuclear cells were isolated by low-density centrifugation (Histopaque 1083, Sigma) and stained with a cocktail of biotinylated lineage antibodies. Biotinylated antibodies were all rat anti-mouse antibodies: anti-CD11b (clone M1/70), anti-B220 (clone RA3-6B2), anti-CD5 (clone 53–7.3), and anti-Gr-1 (clone RB6-8C5) from eBioscience, and anti-Ter119 (clone TER-119) and anti-CD8a (Clone 53–6.7) from Invitrogen. In order to isolate HSCs (gated as Lineage^{neg}Sca1^{+}cKit^{+}CD34$^{-/low}$Flk2^{-}) and ST-HSCs (gated as Lineage^{neg}Sca1^{+}cKit^{+}CD34^{+}Flk2^{-}), lineage depletion was performed to enrich for lineage-negative cells by magnetic separation (Dynabeads, Invitrogen). Lineage-negative cells were stained with anti-Sca-1 (clone D7) (eBioscience), anti-c-kit (clone 2B8) (eBioscience), anti-CD34 (clone RAM34) (eBioscience), anti-CD127 (clone A7R34) (eBioscience), anti-Flk-2 (clone A2F10) (eBioscience), and streptavidin (eBioscience) and sorted using a BD FACSAria III (BD Bioscience).

Data Availability

The data that support the findings of this study are openly available in DRYAD at https://datadryad.org/stash/share/I0GPdlDTkDoBtr8Fmb7OErbL5BmheJyQpAOCF244NvQ, reference number https://doi.org/10.5061/dryad.0zpc866vg. Bulk RNA-seq data are accessible at GSE119466; single-cell RNA-seq at GSE116708; bulk

TWGBS dataset at GSE167891; bulk ATAC-seq dataset at GSE167214.

SUPPLEMENTAL INFORMATION

Supplemental information can be found online at https://doi.org/10.1016/j.stemcr.2021.03.007.

AUTHOR CONTRIBUTIONS

A.G. and M.C.F. designed and performed experiments. A.G performed DNA and RNA-FISH experiments and microscopy analysis. J.P. supported with bioinformatics data analyses. S.K. and D.B.L. performed TWGBS experiments, as well as sequence alignment and methylation calling of TWGBS data. T.L. generated and labeled whole X and Y chromosome paint probes for DNA-FISH experiments. H.K. supported with Pol II Ser2ph antibody preparation. M.A.M. was responsible for bioinformatics analyses of methylome, ATAC-seq, and RNA-seq data. M.C.F. was responsible for all biological sample preparation and processing. A.G., M.A.M., and M.C.F. interpreted experiments and wrote the manuscript. H.G. helped with data interpretation.

ACKNOWLEDGMENTS

We thank Yolanda Markaki at University of California, Los Angeles (UCLA), (United States) for supporting with Xist-RNA-FISH probe preparation. We thank Ali Gawanbacht and Sarah Warth at Ulm University FACS facility for cell sorting support, Angelika Rück for support with confocal microscopy, and the Tierforschungszentrum of the University of Ulm for supporting our animal work. We thank Colin L. Stewart at Developmental and Regenerative Biology, Singapore, for the *Lmna flox* mice. We thank Nadezda Kosyakova (University of Jena, Germany) for supporting with the whole X chromosome DNA-FISH probes preparation and validation. We thank the High Throughput Sequencing unit of the Genomics & Proteomics Core Facility, German Cancer Research Center (DKFZ), for providing excellent next generation sequencing (NGS) services. A.G. was supported by the Marie Curie Ageing Network MARRIAGE. FOR2674 to D.B.L. This work was supported by an Emmy Noether grant, SFB1074 and FOR2674 by the Deutsche Forschungsgemeinschaft (DFG or German Research Foundation) to M.C.F. and by Ministerio de Ciencia, Innovación y Universidades (Spanish Ministry of Science, Innovation and University) PGC2018-102049-B-I00 and RYC2018-025979-I to M.C.F.

Received: June 25, 2020
Revised: March 3, 2021
Accepted: March 4, 2021
Published: April 1, 2021

REFERENCES

Akunuru, S., and Geiger, H. (2016). Aging, clonality, and rejuvenation of hematopoietic stem cells. Trends Mol. Med. *22*, 701–712.

Beerman, I., Bock, C., Garrison, B.S., Smith, Z.D., Gu, H., Meissner, A., and Rossi, D.J. (2013). Proliferation-dependent alterations of the DNA methylation landscape underlie hematopoietic stem cell aging. Cell Stem Cell *12*, 413–425.

Beerman, I., Maloney, W.J., Weissmann, I.L., and Rossi, D.J. (2010). Stem cells and the aging hematopoietic system. Curr. Opin. Immunol. *22*, 500–506.

Brockdorff, N., Bowness, J.S., and Wei, G. (2020). Progress toward understanding chromosome silencing by Xist RNA. Genes Dev. *34*, 733–744.

Brown, C.J., Hendrich, B.D., Rupert, J.L., Lafrenière, R.G., Xing, Y., Lawrence, J., and Willard, H.F. (1992). The human XIST gene: analysis of a 17 kb inactive X-specific RNA that contains conserved repeats and is highly localized within the nucleus. Cell *71*, 527–542.

Buenrostro, J.D., Wu, B., Chang, H.Y., and Greenleaf, W.J. (2015). ATAC-seq: a method for assaying chromatin accessibility genome-wide. Curr. Protoc. Mol. Biol. *109*, 21.29.21–29.

Burke, B., and Stewart, C.L. (2013). The nuclear lamins: flexibility in function. Nat. Rev. Mol. Cell Biol. *14*, 13–24.

Chaumeil, J., Le Baccon, P., Wutz, A., and Heard, E. (2006). A novel role for Xist RNA in the formation of a repressive nuclear compartment into which genes are recruited when silenced. Genes Dev. *20*, 2223–2237.

Chen, C.K., Blanco, M., Jackson, C., Aznauryan, E., Ollikainen, N., Surka, C., Chow, A., Cerase, A., McDonel, P., and Guttman, M. (2016). Xist recruits the X chromosome to the nuclear lamina to enable chromosome-wide silencing. Science *354*, 468–472.

Costanzi, C., and Pehrson, J.R. (1998). Histone macroH2A1 is concentrated in the inactive X chromosome of female mammals. Nature *393*, 599–601.

Croker, B.A., Metcalf, D., Robb, L., Wei, W., Mifsud, S., DiRago, L., Cluse, L.A., Sutherland, K.D., Hartley, L., Williams, E., et al. (2004). SOCS3 is a critical physiological negative regulator of G-CSF signaling and emergency granulopoiesis. Immunity *20*, 153–165.

da Rocha, S.T., and Heard, E. (2017). Novel players in X inactivation: insights into Xist-mediated gene silencing and chromosome conformation. Nat. Struct. Mol. Biol. *24*, 197–204.

Dechat, T., Pfleghaar, K., Sengupta, K., Shimi, T., Shumaker, D.K., Solimando, L., and Goldman, R.D. (2008). Nuclear lamins: major factors in the structural organization and function of the nucleus and chromatin. Genes Dev. *22*, 832–853.

Denkinger, M.D., Leins, H., Schirmbeck, R., Florian, M.C., and Geiger, H. (2015). HSC aging and senescent immune remodeling. Trends Immunol. *36*, 815–824.

Dzierzak, E., and Bigas, A. (2018). Blood development: hematopoietic stem cell dependence and independence. Cell Stem Cell *22*, 639–651.

Engreitz, J.M., Pandya-Jones, A., McDonel, P., Shishkin, A., Sirokman, K., Surka, C., Kadri, S., Xing, J., Goren, A., Lander, E.S., et al. (2013). The Xist lncRNA exploits three-dimensional genome architecture to spread across the X chromosome. Science *341*, 1237973.

Fang, H., Disteche, C.M., and Berletch, J.B. (2019). X inactivation and escape: epigenetic and structural features. Front Cell Dev Biol *7*, 219.

Florian, M.C., Dorr, K., Niebel, A., Daria, D., Schrezenmeier, H., Rojewski, M., Filippi, M.D., Hasenberg, A., Gunzer, M., Scharffetter-Kochanek, K., et al. (2012). Cdc42 activity regulates hematopoietic stem cell aging and rejuvenation. Cell Stem Cell *10*, 520–530.

Florian, M.C., Klose, M., Sacma, M., Jablanovic, J., Knudson, L., Nattamai, K.J., Marka, G., Vollmer, A., Soller, K., Sakk, V., et al. (2018). Aging alters the epigenetic asymmetry of HSC division. PLoS Biol. *16*, e2003389.

Galupa, R., and Heard, E. (2018). X-chromosome inactivation: a crossroads between chromosome architecture and gene regulation. Annu. Rev. Genet. *52*, 535–566.

Geiger, H., de Haan, G., and Florian, M.C. (2013). The ageing haematopoietic stem cell compartment. Nat. Rev. Immunol. *13*, 376–389.

Giorgetti, L., Lajoie, B.R., Carter, A.C., Attia, M., Zhan, Y., Xu, J., Chen, C.J., Kaplan, N., Chang, H.Y., Heard, E., et al. (2016). Structural organization of the inactive X chromosome in the mouse. Nature *535*, 575–579.

Grigoryan, A., Guidi, N., Senger, K., Liehr, T., Soller, K., Marka, G., Vollmer, A., Markaki, Y., Leonhardt, H., Buske, C., et al. (2018). LaminA/C regulates epigenetic and chromatin architecture changes upon aging of hematopoietic stem cells. Genome Biol. *19*, 189.

Guidi, N., and Geiger, H. (2017). Rejuvenation of aged hematopoietic stem cells. Semin. Hematol. *54*, 51–55.

Lebon, J.M., Tam, P.P., Singer-Sam, J., Riggs, A.D., and Tan, S.S. (1995). Mouse endogenous X-linked genes do not show lineage-specific delayed inactivation during development. Genet. Res. *65*, 223–227.

Liu, C., Wang, M., Wei, X., Wu, L., Xu, J., Dai, X., Xia, J., Cheng, M., Yuan, Y., Zhang, P., et al. (2019). An ATAC-seq atlas of chromatin accessibility in mouse tissues. Sci. Data *6*, 65.

Loda, A., and Heard, E. (2019). Xist RNA in action: past, present, and future. PLoS Genet. *15*, e1008333.

Marahrens, Y., Loring, J., and Jaenisch, R. (1998). Role of the Xist gene in X chromosome choosing. Cell *92*, 657–664.

McHugh, C.A., Chen, C.K., Chow, A., Surka, C.F., Tran, C., McDonel, P., Pandya-Jones, A., Blanco, M., Burghard, C., Moradian, A., et al. (2015). The Xist lncRNA interacts directly with SHARP to silence transcription through HDAC3. Nature *521*, 232–236.

Mejia-Ramirez, E., Geiger, H., and Florian, M.C. (2020). Loss of epigenetic polarity is a hallmark of hematopoietic stem cell aging. Hum. Mol. Genet. *29*, R248–r254.

Minajigi, A., Froberg, J., Wei, C., Sunwoo, H., Kesner, B., Colognori, D., Lessing, D., Payer, B., Boukhali, M., Haas, W., et al. (2015). Chromosomes. A comprehensive Xist interactome reveals cohesin repulsion and an RNA-directed chromosome conformation. Science *349*. https://doi.org/10.1126/science.aab2276.

Pandya-Jones, A., and Plath, K. (2016). The "lnc" between 3D chromatin structure and X chromosome inactivation. Semin. Cell Dev. Biol. *56*, 35–47.

Panning, B., and Jaenisch, R. (1998). RNA and the epigenetic regulation of X chromosome inactivation. Cell *93*, 305–308.

Penny, G.D., Kay, G.F., Sheardown, S.A., Rastan, S., and Brockdorff, N. (1996). Requirement for Xist in X chromosome inactivation. Nature *379*, 131–137.

Pinheiro, I., and Heard, E. (2017). X chromosome inactivation: new players in the initiation of gene silencing [version 1; peer review: 2 approved]. F1000Res. *6*, 344.

Plath, K., Mlynarczyk-Evans, S., Nusinow, D.A., and Panning, B. (2002). Xist RNA and the mechanism of X chromosome inactivation. Annu. Rev. Genet. *36*, 233–278.

Politz, J.C., Scalzo, D., and Groudine, M. (2013). Something silent this way forms: the functional organization of the repressive nuclear compartment. Annu. Rev. Cell Dev. Biol. *29*, 241–270.

Rossi, D.J., Bryder, D., and Weissman, I.L. (2007). Hematopoietic stem cell aging: mechanism and consequence. Exp. Gerontol. *42*, 385–390.

Sahakyan, A., Kim, R., Chronis, C., Sabri, S., Bonora, G., Theunissen, T.W., Kuoy, E., Langerman, J., Clark, A.T., Jaenisch, R., et al. (2016). Human naive pluripotent stem cells model X chromosome dampening and X inactivation. Cell Stem Cell *20*, 87–101.

Sahakyan, A., Yang, Y., and Plath, K. (2018). The role of xist in X-chromosome dosage compensation. Trends Cell Biol. *28*, 999–1013.

Savarese, F., Flahndorfer, K., Jaenisch, R., Busslinger, M., and Wutz, A. (2006). Hematopoietic precursor cells transiently reestablish permissiveness for X inactivation. Mol. Cell Biol. *26*, 7167–7177.

Snoeck, H.W. (2013). Aging of the hematopoietic system. Curr. Opin. Hematol. *20*, 355–361.

Solovei, I., Kreysing, M., Lanctot, C., Kosem, S., Peichl, L., Cremer, T., Guck, J., and Joffe, B. (2009). Nuclear architecture of rod photoreceptor cells adapts to vision in mammalian evolution. Cell *137*, 356–368.

Solovei, I., Wang, A.S., Thanisch, K., Schmidt, C.S., Krebs, S., Zwerger, M., Cohen, T.V., Devys, D., Foisner, R., Peichl, L., et al. (2013). LBR and lamin A/C sequentially tether peripheral heterochromatin and inversely regulate differentiation. Cell *152*, 584–598.

Sun, D., Luo, M., Jeong, M., Rodriguez, B., Xia, Z., Hannah, R., Wang, H., Le, T., Faull, K.F., Chen, R., et al. (2014). Epigenomic profiling of young and aged HSCs reveals concerted changes during aging that reinforce self-renewal. Cell Stem Cell *14*, 673–688.

Taiwo, O., Wilson, G.A., Emmett, W., Morris, T., Bonnet, D., Schuster, E., Adejumo, T., Beck, S., and Pearce, D.J. (2013). DNA methylation analysis of murine hematopoietic side population cells during aging. Epigenetics *8*, 1114–1122.

van Steensel, B., and Belmont, A.S. (2017). Lamina-associated domains: links with chromosome architecture, heterochromatin, and gene repression. Cell *169*, 780–791.

Wang, A.S., Kozlov, S.V., Stewart, C.L., and Horn, H.F. (2015). Tissue specific loss of A-type lamins in the gastrointestinal epithelium can enhance polyp size. Differentiation *89*, 11–21.

Wilson, K.L., and Berk, J.M. (2010). The nuclear envelope at a glance. J. Cell Sci. *123*, 1973–1978.

Yildirim, E., Kirby, J.E., Brown, D.E., Mercier, F.E., Sadreyev, R.I., Scadden, D.T., and Lee, J.T. (2013). Xist RNA is a potent suppressor of hematologic cancer in mice. Cell *152*, 727–742.

Yokomizo, T., and Dzierzak, E. (2010). Three-dimensional cartography of hematopoietic clusters in the vasculature of whole mouse embryos. Development *137*, 3651–3661.